# Effective elastin-like recombinamers coating on poly(vinylidene) fluoride membranes for mesenchymal stem cell culture

*Maria Guillot-Ferriols[1, 2] \*, Ana del Barrio[3], Carlos M. Costa[4,5],*

*Senentxu Lanceros Méndez[4,6,7], José Carlos Rodríguez-Cabello[2,3],*

*José Luis Gómez Ribelles[1,2], Mercedes Santos[2,3], Gloria Gallego Ferrer[1,2]\**

[1] Centre for Biomaterials and Tissue Engineering (CBIT), Universitat Politècnica de València, 46022 Valencia, Spain

[2] Biomedical Research Networking Center on Bioengineering, Biomaterials and Nanomedicine (CIBER-BBN), Valencia, Spain

[3] BIOFORGE Group, Centro de Investigación Científica y Desarrollo Tecnológico, Universidad de Valladolid, 47011, Valladolid, Spain

[4] Centre/Department of Physics, Universidade Do Minho, 4710-058 Braga, Portugal

[5] Centre of Chemistry, Universidade Do Minho, 4710-058 Braga, Portugal

[6] BCMaterials, Basque Center for Materials, Applications and Nanostructures, UPV/EHU Science Park, 48940 Leioa, Spain

[7] IKERBASQUE, Basque Foundation for Science, 48013 Bilbao, Spain.

**ABSTRACT**

Bone's inherent piezoelectricity is a key factor regulating bone's growth and mesenchymal stem cell (MSCs) fate towards the osteogenic lineage. For that purpose, the piezoelectric polymer poly(vinylidene) fluoride (PVDF) was used to manufacture electroactive membranes by means of non-solvent induced phase separation (NIPS), producing porous membranes with approximately 90 % of γ-phase for MSCs culture. Porous surface and PVDF hydrophobicity combination hinder cell adhesion requiring a coating to improve cell culture conditions. Layer-by-layer (LbL) methodology was used for the deposition of elastin-like recombinamers (ELRs), containing RGD sequences, applying the click cross-linking chemistry. ELRs potential was confirmed comparing traditional fibronectin adsorption with ELRs LbL on PVDF electroactive membranes. Porcine bone marrow MSCs preferred ELRs coated surfaces, enhancing initial cell adhesion and improving proliferation after 7 days. These findings lead to new possibilities for electro-mechanical stimulation of MSCs on PVDF substrates to study cell differentiation towards the osteogenic linage.

**KEYWORDS**: Poly(vinylidene) fluoride, piezoelectricity, elastin-like recombinamers, RGD, layer-by-layer, mesenchymal stem cells

## 1. INTRODUCTION

Poly(vinylidene) fluoride (PVDF) is a piezoelectric semi-crystalline polymer which can crystallize into five polymorphs, α, β, γ, δ and ε. Chain conformations, all trans (TTT) planar zigzag and $T_3GT_3G$ for β and γ phases respectively [1], and electronegativity difference between fluorine and

hydrogen atoms create a net dipole moment in these polymorphs, conferring them electroactive properties [2].

PVDF has been proposed as a candidate for bone tissue engineering (TE) approaches, due to its capacity to produce a surface charge variation when a mechanical input is applied [3] reproducing bone's inherent piezoelectricity discovered by Fukada and Yasuda [4]. This mechanism is hypothesized to be involved in bone capacity to adapt to mechanical stress and tissue regeneration [5]. It has been demonstrated that electro-mechanical stimulation enhances cell viability, proliferation and differentiation on osteogenic progenitors [6–8].

The interest in using PVDF in bone TE lies in the presence of the electroactive phases, which can be obtained during the manufacturing process. The $\alpha$-phase of PVDF is the most commonly obtained, as crystallization from the melt results in this polymorph [9]. $\beta$-phase can be produced by uniaxial stretching of the $\alpha$ polymorph [10], which is a two-step process. On the other hand, crystallization below 70 ºC using polar solvents as dimethylformamide allows obtaining both $\beta$ and $\gamma$ electroactive phases [11,12], reducing the manufacturing process to a single step [13], and allowing the manufacturing of the support in complex shapes.

Non-solvent induced phase separation (NIPS) is a technique compatible with the aforementioned parameters. It consists on the precipitation of the polymer casted on a surface by immersing it in a coagulation bath containing a non-solvent [14,15]. Different topographies and diverse electroactive contents can arise depending on the applied manufacturing conditions [16]. It is a reliable, cost-effective and simple method for the production of electroactive PVDF supports for cell culture [17].

When considering PVDF for biological applications, the modification of the surface properties is necessary to control cell behavior due to its high hydrophobicity [18]. Specifically, for culturing cells

with osteogenic characteristics fibronectin adsorption is usually applied to enhance its initial adhesion and proliferation [8,19,20]. Nonetheless, fibronectin has proven to be ineffective in highly porous PVDF supports regarding mesenchymal stem cell (MSCs) adhesion [21].

Elastin-like recombinamers (ELRs) have arisen as suitable biomolecules for biomimetic polymer coatings that include specific biofunctional sequences. ELRs are synthetic elastin-inspired polypeptides, produced by DNA recombinant technologies, formed by repetitive sequences comprising the most widely used pentapeptide domain Val-Pro-Gly-X-Gly (VPGXG), being X any natural or modified amino acid, with the exception of L-proline [22]. ELRs can be engineered to incorporate bioactive sequences, conferring them specific properties regarding cell attachment, proliferation and differentiation [23]. In this sense, the sequence Arg-Gly-Asp (RGD), found in a number of extracellular matrix proteins, is known for mediating cell attachment and spreading[24,25]. This domain was one of the first bioactive motifs introduced at the ELR main chain [26] and applied as substrate coating, showing an increase in cell affinity [27]. Besides mediating cell adhesion, RGD sequence has proven to be involved in MSCs differentiation towards the osteogenic lineage [28–31].

On the other hand, biocompatible ELR click hydrogels can be obtained by interchain crosslinking via catalyst-free Hüisgen 1,3-dipolar cycloaddition under physiological conditions in an atom economy, mild and cell-friendly process [32]. These click hydrogels are outstanding candidates for tissue engineering [33], in general, and as layer-by-layer (LbL) stable and biomimetic coatings, in particular, with increased adhesion and proliferation when RGD is incorporated, establishing the bases for future biomedical applications [34].

In this study, we combined electroactive PVDF membranes, produced by NIPS, with ELRs containing RGD sequences deposited on their surface by LbL technique applying the click

crosslinking approach, as cell culture supports for *in vitro* mesenchymal stem cell culture. Effectiveness of ELRs LbL coating on PVDF electroactive supports was compared with a traditional fibronectin adsorption using porcine bone marrow MSCs. The obtained results on cell proliferation on the ELR coated materials make them promising candidates for electro-mechanical stimulation approaches.

## 2. EXPERIMENTAL

### 2.1 Electroactive membrane preparation

Poly(vinylidene) fluoride membranes were produced using the non-solvent induced phase separation technique. For that purpose, a 20 % w/v PVDF solution (Solef® 6010 PVDF Homopolymer, Solvay) in dimethylformamide (DMF) (Scharlab, synthesis grade) was prepared. The solution was magnetically stirred at 60 ºC until complete dissolution of the polymer. Prior to membrane preparation, the solution was kept non-stirred for 30 min, to remove air bubbles. After this time, the solution was spread on a glass plate using a casting knife with a height of 750 μm. The plate was immersed in a coagulation bath containing absolute ethanol (Scharlab) at 25 ºC for 1 h. After complete precipitation, the membranes were washed in deionized water to remove the excess of ethanol and remaining traces of DMF. Then, they were washed under agitation for 24 h, with a water exchange every two hours. Once washed, the membranes were frozen at -80 ºC and lyophilized for 24 h.

**2.2 Membrane characterization**

**2.2.1  Morphological analysis**

Membrane surface and cross-section morphology were analysed by means of Field Emission Scanning Electron Microscopy (FESEM). Samples were coated with platinum following a standard sputtering protocol for 90 s (JFC 1100, JEOL, Japan) and visualized in an Ultra 55 microscope (Zeiss). Accelerating voltage was 2 kV. Surface spherulite diameter was measured using ImageJ software (National Institutes of Health, Bethesda, Maryland, USA). Three different membranes from three different batches were analysed, considering 100 spherulites per sample.

ELRs deposition by layer-by-layer technique was also confirmed acquiring images from the coated surface and the cross-section using FESEM applying an accelerating voltage of 1 kV.

**2.2.2  Porosity measurements**

Porosity of the developed membranes was measured filling the pores with ethanol and applying equations (1) and (2):

$$(1) \qquad V_{pores} = \frac{m_{wet} - m_{dry}}{\rho_{ethanol}}$$

$$(2) \qquad \emptyset = \frac{V_{pores}}{V_{pores} + V_{PVDF}}$$

where $m_{wet}$ and $m_{dry}$ correspond to the weight of the membranes before and after their immersion in ethanol, respectively. $\rho_{ethanol}$ is the ethanol density, which is 0.789 g/cm³. PVDF volume ($V_{PVDF}$) was calculated with the dry weight of the membrane and assuming a density of 1.775 g/cm³.

Three replicates per sample were measured from three different samples produced in different preparations. Porosity ($\emptyset$) was expressed as mean ± standard deviation.

### 2.2.3 Analysis of the electroactive phases

Determination of the electroactive phase content present in the membranes was assessed by Fourier Transformed Infrared Spectroscopy (FTIR). Benz and Euler [35] defined a simple method to quantify PVDF crystalline phases present in a sample, especially when the presence of γ-phase is remarkable. Different phases were identified by its representative absorption bands, 762 cm⁻¹ for α, 1279 cm⁻¹ for β and 835 cm⁻¹ for γ. Since absorption band at 835 cm⁻¹ has contributions from β, γ and the amorphous phase, the fraction of γ -phase (F(γ)) present in the sample can be calculated applying the following equations [35,36]:

$$(3) \qquad F(\gamma) = \frac{X_\gamma}{X_\gamma + X_\alpha}$$

$$(4) \qquad A_{835} = (K_\gamma^{835} X_\gamma + K_\beta^{835} X_\beta + K_{am}^{835}(1 - X_{total}))t$$

$$(5) \qquad A_{762} = K_\alpha^{762} X_\alpha \, t$$

$$(6) \qquad\qquad A_{1279} = K_{\beta}^{1279} X_{\beta}\, t$$

Where $X_{\alpha}$ and $X_{\gamma}$ are the fraction of $\alpha$ and $\gamma$ phases and $A_{\alpha}$ and $A_{\gamma}$ are their absorptions at 762 and 835 cm$^{-1}$, respectively. K are the characteristic absorption coefficients at the characteristic wavenumbers of each one of the phases ($K_{\alpha}^{762} = 0.365$ µm$^{-1}$, $K_{\gamma}^{835} = 0.15$ µm$^{-1}$, $K_{am}^{835} = 0.0259$ µm$^{-1}$ [35]), $X_{total}$ is the total crystallinity of the sample, and $t$ is its thickness. In this work, the contribution from $\beta$-phase to equation 4 is negligible since there is no presence of the peak at 1279 cm$^{-1}$. Also, the high crystallinity of the membranes makes $K_{\gamma}^{835} X_{\gamma}$ much larger than $K_{am}^{835}(1 - X_{total})$. Moreover $K_{\gamma}^{835}$ is five times larger than $K_{am}^{835}$. In this case, Eq. (3) can be reduced to:

$$(7) \qquad\qquad F(\gamma) = \frac{A_{835}}{\left(\dfrac{K_{\gamma}^{835}}{K_{\alpha}^{762}}\right) A_{762} + A_{835}}$$

Measurements were taken using an ALPHA FTIR spectrometer (Bruker) in ATR mode from 4000 to 400 cm$^{-1}$ at a wavelength resolution of 4 cm$^{-1}$. Three different membranes from three different batches were analysed. The percentage of electroactive content was expressed as mean ± standard deviation.

### 2.2.4 Membrane's crystalline content

Differential Scanning Calorimetry was used to determine the crystallinity degree ($X_c$) of the produced PVDF membranes as well as their melting temperature. Samples were scanned in a DSC Pyris 1 (PerkinElmer) calorimeter, previously encapsulated in aluminium pans. Scans were performed from 0 °C to 200 °C at a heating range of 20 °C/min in a dry nitrogen atmosphere.

$X_c$ was determined by means of the following equation [35–37]:

$$(8) \qquad X_c = \frac{\Delta H_m}{\Delta H_{100}} \times 100$$

$\Delta H_m$ is the melting enthalpy of the PVDF membranes measured in DSC and $\Delta H_{100}$ is the melting enthalpy for a 100% crystalline sample of pure PVDF, which value is 104.7 J/g [38]. Three different membranes from three different batches were analysed. The crystallinity degree and melting temperature were expressed as mean ± standard deviation.

### 2.2.5 Poling method and piezoelectric coefficient evaluation

The porous membranes were poled by the contact method, with the polymer membranes placed inside a silicone oil bath to prevent electrical breakdown. On both membrane surfaces, aluminium adhesive tape was used as electrode materials. Polarization conditions were optimized to a final electric field of ~10 kV at a constant current of 10 µA during 1 h at a temperature of 120 ºC.

After the poling time, the membranes were cooled down to room temperature under the application of the electric field.

The piezoelectric $d_{33}$ response was analysed with a Wide Range d33-meter (Model 8000, APC Int Ltd).

### 2.3 ELRs deposition on PVDF membranes

#### 2.3.1 Biosynthesis and purification of ELRs

ELRs were bioproduced by using genetic engineering technology and purified by Inverse Transition Cycling (ITC) [39,40], exploiting their thermosensitive behaviour. The ELR obtained was named as HRGD and its amino-acid sequence was:

HRGD: MGSSHHHHHHSSGLVPRGSH-MESLLP-{[(VPGIG)2(VPGKG)(VPGIG)2]2-AVTGRGDSPASS- [(VPGIG)2(VPGKG)(VPGIG)2]2]}6-V

The polymer contained VPGKG pentapeptide located uniformly along the main chain that will enable further chemical modification through the ε-amine group of lysines. HRGD biopolymer also contained the peptide loop found in human fibronectin, carrier of RGD sequence specific for cell adhesion. The purity and chemical characterization of ELR was verified by sodium dodecyl sulphate polyacrylamide gel electrophoresis (SDS–PAGE), matrix-assisted laser desorption/ionization time-of-flight (MALDI-ToF) mass spectrometry, amino acid composition analysis, differential scanning calorimetry (DSC) and nuclear magnetic resonance (NMR) [41]. ^{1}H-NMR spectroscopy and MALDI-ToF-mass spectrometry were carried out in the laboratory of Instrumental Techniques (LTI) of the Research Facilities of the University of Valladolid.

#### 2.3.2 ELRs chemical modification

ELRs were chemically modified to carry cyclooctyne or azide groups at the lateral chain obtaining the corresponding modified biopolymers named RGD-CO for that bearing cyclooctyne

derivatization and named RGD-N3 for that with azide groups. The biopolymers chemical functionalization was carried out by modification of ε-amine groups, as previously described [32].

To modify HRGD with a cyclooctyne group, the ELR was solved in DMF (Sigma), at final concentration of 0.05 g/mL and at room temperature under inert atmosphere. Then, bicyclo [6.1.0] non-4-yn-9-yl-methyl N-succinimidyl carbonate (0.6 eq, Mw 291.30 mg/mmol, GalChimia, A Coruña, Spain) dissolved in DMF was added to the ELR solution at final concentration of 3.3 mg/mL. The resulting mixture was stirred for 48 h at room temperature in argon atmosphere. The modified RGD-CO was purified by precipitation with diethyl ether. The resulting white solid was washed with acetone (3 times) and dried under reduced pressure. The solid was re-dissolved in cold ultrapure MQ water at 4 °C, dialyzed against MQ water, filtered through 0.22 μm filters (Nalgene) and the sterile solution was freeze-dried prior to storage.

Following the same procedure, HRGD was modified to bear an azide group. This time 2-Azido ethyl (2,5-dioxopyrrolidin-1-yl) carbonate (0.6 eq, Mw 228.17 mg/mmol, GalChimia, A Coruña, Spain) was dissolved in DMF and, then, was added to the ELR solution at final concentration of 1.3 mg/mL. Purification of RGD-N3 was carried out as previously described.

The modified biopolymers RGD-CO and RGD-N3 were characterized by NMR, MALDI-ToF and Fourier transform infrared spectroscopy (FTIR-ATR) (Supporting information). MALDI-ToF and ^{1}H-NMR (in DMSO-d6) enabled us to quantify the degree of lysine modification.

### 2.3.3 Layer-by-Layer procedure for ELR-covered PVDF membranes

PVDF membranes cut into squares with sides of one centimetre were used as substrate for ELR coating. The squared surfaces were marked with a signal placed on the opposite face to the cell

culture. Firstly, these substrates were activated by plasma treatment. So, once the membrane pieces were placed into the chamber and vacuum was generated (P=600 mTorr), argon plasma flow of 20 mL/min created at a high radiofrequency (29.6 W) passed through the samples during the adequate time. Four different times were studied (1, 5, 20 and 30 minutes) to optimize plasma treatment activation time.

Secondly, different ELRs solution concentrations as well as the immersion order were studied to achieve the best coating for cellular assays. The ELRs modified with either cyclooctyne or azide groups were dissolved at 10 or 25 mg/mL, depending on the corresponding assay, in water at 4 ºC overnight and kept at this temperature in separate containers during their use. The activated PVDF membranes, selecting the optimized plasma treatment protocol, were sequentially immersed in the ELR solutions, using either RGD-N3 or RGD-CO as the first layer, during two seconds and left to dry for five minutes between dippings generating the first bilayer, this process was repeated twice. After being left to dry for 45 minutes, the membranes were freeze-dried.

### 2.3.4 Characterization of ELR-covered PVDF membranes

As process control, the non-activated, activated and the final biofunctionalized membranes were evaluated by contact angle measurements determined by a sessile drop method using a Data Physics OCA20 system instrument equipped with an adapted CCD video camera. The proper coating performance was analysed by Fourier transform infrared spectroscopy (FTIR-ATR) using a Bruker TENSOR 27 acquiring 64 scans between 500-4000 cm$^{-1}$, comparing the spectra of the biofunctionalized membranes with the non-coated ones. Membrane surfaces and cross-section morphology was analysed by FESEM as previously described in section 2.1.1.

## 2.4 Cell culture assays

Porcine bone marrow mesenchymal stem cells (pMSCs) were used to study cell response regarding proliferation. pMSCs were expanded in basal medium containing Dulbecco's modified Eagles medium (DMEM) high glucose (4.5 g/L) with GlutaMAX$^{TM}$ (Gibco), 10% (v/v) Foetal Bovine Serum, FBS (Gibco), 100 U/mL penicillin-100 µg/mL streptomycin, P/S (Life technologies), and 5 ng/mL of Fibroblast Growth Factor 2, FGF-2 (Eurobio), at 37 ºC in a humidified atmosphere with 5 % $CO_2$. All the experiments were performed in passage 5.

After choosing the best layer-by-layer protocol for deposition of ELRs, coated (PVDF + ELRs) and non-coated membranes (PVDF), were cut in 8 mm disks, to fit the bottom of a 48 well plate. Samples were sterilized by UV for 20 minutes on each side. After this, membranes were washed in ethanol 70% (v/v) for 15 minutes under shacking. To eliminate possible traces of ethanol, they were washed 6 times in Dulbecco's Phosphate Buffered Saline, DPBS (Sigma-Aldrich).

Glass slides, used as controls, were sterilized by sonication in ethanol for 10 minutes and after that they were exposed to UV for 20 minutes on each side.

After sterilization, non-coated membranes and glass slides were incubated with a solution of fibronectin from human plasma (Sigma-Aldrich; 20 µg/mL) for 1 hour at room temperature. Fibronectin coating was used to compare the effectiveness of ELRs deposition by layer-by-layer compared to a more traditional protein adsorption. After fibronectin coating, samples were washed twice with DPBS to remove non-adsorbed fibronectin.

Samples were placed in a 48 well plate, 3 replicates per group, and silicon rings were used to prevent the membranes from floating inside the wells, glass slides included. Basal medium without FBS nor FGF-2 was added to the wells to condition the membranes before cell seeding.

12 h before cell seeding, cells were starved in basal medium containing 1 % (v/v) FBS to synchronize cell cycle. To study cell proliferation cells were seeded at a density of $8 \times 10^3$ cells/cm$^2$ in basal medium without FBS to promote cell adhesion either to fibronectin or ELRs containing RGD sequences. 100 μL containing the required number of cells were deposited on top of each sample, inside the silicon rings. 3 h later, after cell attachment was produced, the required volume of basal medium and FBS for a final concentration of 10% (v/v) were added to each well.

Medium was changed every 2 or 3 days. After 24 h, 3 and 7 days samples were fixed using a 4 % (v/v) paraformaldehyde solution (Panreac) for 20 minutes.

Initial adhesion and proliferation studies were carried out by means of staining cell cytoskeleton and nuclei. After fixation, samples were permeabilized and blocked in 1% (w/v) bovine serum albumin (BSA; Sigma-Aldrich) solution in DPBS/0.1% (v/v) Tween-20 (Sigma-Aldrich) for 1 h at room temperature. Subsequently, they were incubated with Alexa Fluor Phalloidin 488 (1:100 Fisher Scientific) for 2 hours in a humidified chamber. After washing the samples 3 times with DPBS/0.1% (v/v) Tween-20 (Sigma-Aldrich), PVDF membranes were treated with Sudan Black B solution following the protocol described by Morales-Román et al. [21]. PVDF autofluorescence hinders image acquisition and cell counting, so Sudan Black B treatment is necessary to obtain quality images of the cells. After that, samples were washed 3 times with DPBS and incubated for 20 minutes with DAPI (1:200; Sigma-Aldrich) in mounting medium.

Four representative areas of each sample were studied, acquiring images with a fluorescence microscope (Nikon Eclipse 80i). Images were analysed using ImageJ software (National Institutes of Health, Bethesda, Maryland, USA). Two independent assays were carried out, with three replicates per group. Cell number was normalized by the initial cell seeding density and expressed as relative cell proliferation (Log2 fold change), each unity corresponding to a duplication in the cell population.

### 2.5 Statistical analysis

Statistical analysis was performed using SPSS Software. Two-way ANOVA analysis was applied for homogeneous groups, after checking homoscedasticity by Levene test. A 95% confidence interval was set to accept significant differences between groups ($p\text{-value} < 0.05$).

## 3. RESULTS AND DISCUSSION

### 3.1 Membrane characterization

PVDF membranes were produced by non-solvent induced phase separation (NIPS) in an ethanol bath at 25 ºC. The election of the non-solvent in the coagulation bath, among a wide variety of parameters, is instrumental in membrane morphology formation. Being PVDF a semi-crystalline polymer, its precipitation during this process is determined by two events, liquid-liquid demixing and solid-liquid demixing, associated with crystallization [16]. The presence of ethanol in the coagulation bath, a soft non-solvent, reduces the solvent-nonsolvent exchange, allowing crystallization, a slower process, before liquid-liquid demixing takes place.

Membranes' structure and morphology was characterized by FESEM, as shown in figure 1. Figure 1 (b) shows symmetrical PVDF membranes, with both porous surfaces on the top (Figure 1 (a)) and bottom parts (images of the bottom surface are not displayed). The use of soft solvents in the coagulation bath gives rise to symmetric membranes, without the characteristic presence of finger-like structure or macrovoids present in water-bath produced membranes [42]. Crystallization is produced before crossing the binodal line, allowing crystalline globules to grow and coalesce [11].
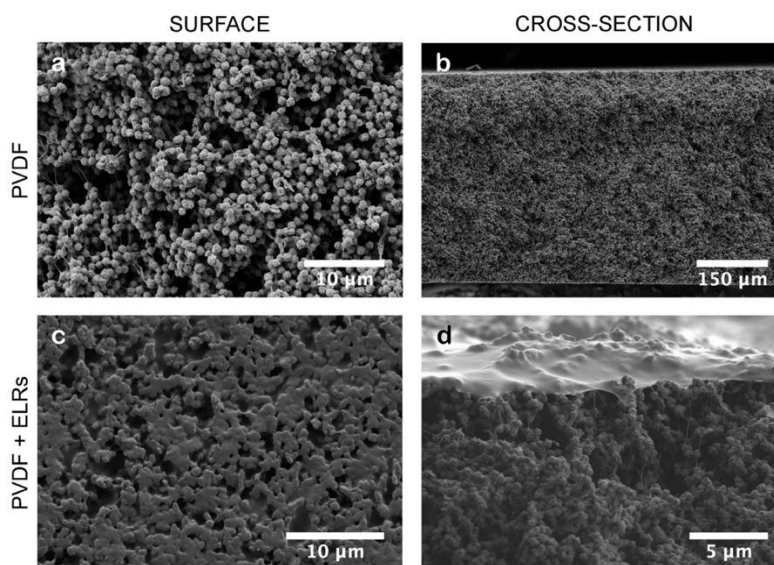


**Figure 1**. Surface and cross-section FESEM images of PVDF membranes produced by non-solvent induced phase separation before ELRs deposition by layer-by-layer (a and b) and after (c and d).

Surface topography is formed by a particulate-like morphology, composed by PVDF globules or microbeads. These structures measure $1.1 \pm 0.2$ μm, in agreement with previous results reported by Lin et al [43]. Pagliero et al. [11] manufactured PVDF membranes in ethanol baths varying the concentration of PVDF in the initial solution. Highly concentrated solutions of PVDF (above 14 % w/v) gave rise to smaller spherulites, compared with the ones obtained from diluted solutions. Polymer concentration rise in the initial solution increased solution viscosity, favouring PVDF

entanglements, restraining chain mobility and reducing spherulites growth. Moreover, a more compact interconnected network could be observed, as is the case for the present membranes using 20 % w/v PVDF shown in figure 1 (a). These globules are connected to each other by fibrils, probably with the thickness of one or more folded lamellae, as previously reported by Lin et al.[44].

Porosity was determined filling the pores of the membrane with ethanol and applying equations 1 and 2. Ethanol was chosen since PVDF high hydrophobicity hinders pore filling with water, underestimating pore volume, as stated by Morales-Román et al.[21]. PVDF membranes produced by NIPS in ethanol coagulation bath displayed a porosity of $81.7 \pm 0.5$ %.

Fourier transformed infrared spectroscopy (FTIR) has proven to be a valid method to identify and quantify PVDF polymorphs present in different samples, applying the aforementioned equations in materials and methods section. Martins et al. [45] reviewed the characteristic absorption bands of the most common crystalline phases $\alpha$, $\beta$ and $\gamma$. The non-electroactive $\alpha$-phase is defined by the wavenumbers at 532, 614, 762, 795, 855, 976 cm$^{-1}$, being the most representative and the one used to calculate its fraction at 762 cm$^{-1}$. Bands at 445, 510, 840 and 1279 cm$^{-1}$ are used to identify $\beta$-phase, while 431, 512, 812, 835 and 1234 cm$^{-1}$ are the ones for $\gamma$-phase. Identification of electroactive $\beta$ and $\gamma$ phases using FTIR-ATR has been a matter of debate in the last years, since their similar structure provides characteristic absorption bands, which are a superposition of both phases. Among those bands, 1279 and 1234 cm$^{-1}$ can be used to unequivocally identify them, since $\beta$ and $\gamma$ contributions, respectively, are unique at these wavenumbers.

Representative FTIR-ATR spectrum of PVDF membranes is displayed in figure 2 (a). $\alpha$-phase characteristic bands at 614, 762 and 976 cm$^{-1}$ are exhibited, as highlighted in the graph. Surprisingly, no $\beta$-phase peaks are present, noticing the absence of the one at 1279 cm$^{-1}$. However,

most of the γ-phase characteristic bands can be found in the sample, including 431, 835 and 1234 cm$^{-1}$. Since 1234 cm$^{-1}$ tends to appear as a shoulder, 835 cm$^{-1}$ is used to quantify the percentage of γ-phase present in the membranes [35–37,46]. The absence of β-phase peaks makes its contribution to this 835 cm$^{-1}$ negligible, allowing to apply equation 7 to obtain γ-phase fraction. The percentage of γ-phase is 93.3 ± 1.4 %, with just a small contribution of α-phase (6.6 ± 1.4 %). Obtaining γ-phase is more difficult than β and traditionally it has only been achieved by isothermal crystallization at extremely high temperatures and at slow cooling rates [47]. The addition of fillers [37] and crystallization under vacuum [48] have also produced PVDF supports in this electroactive phase. Some authors have also reported its obtaining by means of NIPS [12,36]. Highly polar solvents, as dimethylformamide or dimethylacetamide, favour crystallization in trans phases due to their interaction with the polymer, rotating the C-F bond around the C-C bonds of chain backbone [49]. In other words, membranes' γ-phase is produced by the dipole rotation (α to γ) induced by solvent polarity. It has been proved that the presence of alcohols in the coagulation bath favours the interaction between its -OH groups and the solvent, DMF [36]. This phenomenon allows partially the rotation back to α conformation, leading to the low contribution to the sample crystalline content.
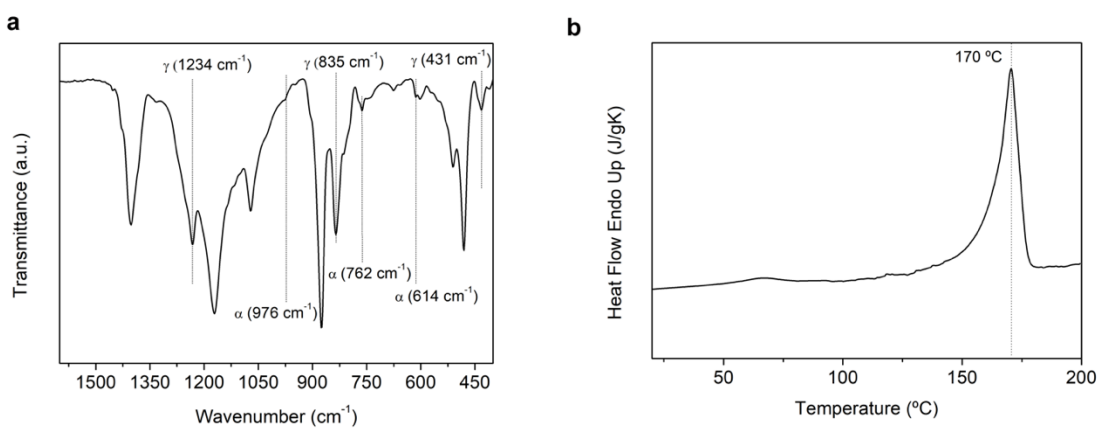
**Figure 2.** Representative (a) FTIR-ATR spectrum and (b) DSC curve of PVDF membranes produced by non-solvent induced phase separation.

Membrane electroactive potential was confirmed measuring the piezoelectric $d_{33}$ response, after poling the samples. Corona discharge poling could not be used due to membrane high porosity, up to 80 %, which produced electrical breakdown, so direct contact method filling the membrane pores with silicone oil to prevent electric breakdown was used. Immediately after the polarization process, the $|d_{33}|$ (values are negative, as typical for PVDF) response varied between 3 and 6 pC/N, depending of the measurement specific place of the porous membranes.

Further, these piezoelectric membranes were coupled to a readout electronic circuit [50] in order to observe the voltage generated under cycling pressure solicitation by gentle finger pressing and releasing. Figure 3 shows the voltage generated when the membrane is repeatedly pressed and released.
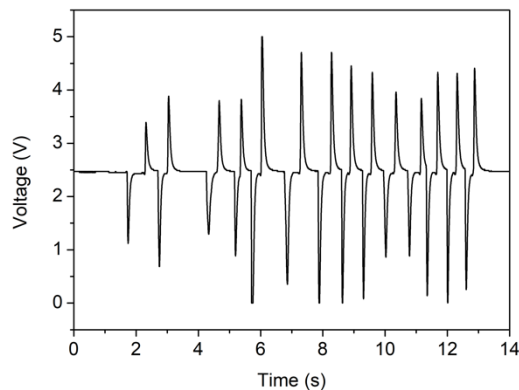


**Figure 3.** Voltage generation through the piezoelectric PVDF membrane under cycling pressing and releasing events.

It is observed a stable voltage generation under mechanical deformation originated by gentle finger pressing, compatible to the measured piezoelectric response.

Despite the important efforts to elucidate bone piezoelectric coefficients, published data show notable disparity. Piezoelectric coefficients attributed either to bone or tendons, containing oriented collagen fibers, usually differ in more than one order of magnitude [3,51–54]. Halperin et al. [55] studied the piezoelectric coefficients in dry and wet human bone and concluded that the piezoelectric coefficient varies in the range 7 to 8 pC/N, in consonance with the results published by other authors [51,53]. Even though γ-PVDF electroactive response is lower than the one of β-PVDF, the obtained piezoelectric coefficient is in the same order of magnitude than the ones reported by the aforementioned authors. This fact reveals that γ-PVDF membranes are suitable candidates for future mesenchymal stem cell differentiation approaches.

Thermal properties and crystallinity degree of the PVDF membranes were assessed by differential scanning calorimetry. The melting endotherm obtained at a heating range of 20 ºC/min is shown in figure 2 (b). The melting peak, indicating the melting temperature ($T_m$) of the PVDF membranes, appears at 169.4 ± 1.2 ºC. Even though γ polymorph displays a $T_m$ around 8 ºC higher than α and β, as described by Gregorio [9], the obtaining of this polymorph is based on isothermal crystallization at 166 ºC. Higher crystallization temperatures lead to higher crystallite sizes, increasing the melting temperature. PVDF membranes here presented were obtained at 25 ºC which resulted in a lower melting temperature, in agreement with the data obtained by Chang et al [36,46]. Chang et al. manufactured PVDF membranes by NIPS technique using different solvents and alcohols in the coagulation bath, obtaining mostly γ-phase membranes with melting temperatures around 165-170 ºC.

Membrane's crystallinity degree was obtained applying equation 8. $X_c$ is 65 ± 1 % for PVDF membranes. This data confirms that liquid-liquid demixing is delayed by the use of non-solvents

due to the reduction of solvent-nonsolvent exchange rate. This delay allowed crystallization to take place, including nucleation and spherulite growth, producing membranes with a high percentage of crystalline phase within its structure.

### 3.2 ELRs deposition by layer-by-layer technique

Surface fibronectin adsorption is a common technique when using PVDF as cell culture support, since PVDF hydrophobicity hinders initial cell adhesion. However, using a different approach, as layer-by-layer ELR deposition, a complete and stable coating of the surface can be achieved. Strong covalent bonds between layers are formed assuring a permanent coating that can be used in tissue engineering field. This ELRs coating is considered cell-friendly because of ELRs biocompatibility, as demonstrated in previous works [56], and of their copper-free click cross-linking between layers . This click methodology involves the 1,3-dipolar cycloaddition of an azide and an especially active alkyne group, such as cyclooctyne (based on annular tension), allowing the reaction to take place without needing a catalyst [32] and applying atom economy.

A first study comprising optimization and characterization of diverse coating conditions was performed. Initially, membrane activation time using plasma treatment was optimized and subsequently RGD-N3 and RGD-CO solution concentration and the deposition order of the first layer was studied. Once the optimal conditions were obtained, PVDF membranes were coated for cell culture tests depositing two bilayers of the aforementioned ELRs.

The activation of PVDF membranes was carried out by a simple, clean and effective method such as plasma treatment. The argon plasma flow (20 mL/min) was passed through a vacuum chamber (600 mTorr) and several time periods (1, 5, 20 and 30 minutes) were applied over the samples deposited inside. The control of this step was performed by measuring the contact angle of a water

drop on the PVDF membrane surface. The small difference in contact angle between non-activated (133.2±1.4°) and activated membranes at different times (non-significant differences in contact angle values around 120°) showed a soft decrease in hydrophobicity despite plasma treatment. However, the activation, in all time periods tested, was enough to allow immersing the samples in aqueous solutions for the ELRs coating. To avoid membrane damage, the minimum activation time of 1 minute was chosen for the LbL process.

Before membrane coating, ELRs were chemically modified in order to be carriers of azide and cyclooctyne functional groups, giving rise to RGD-N3 and RGD-CO, respectively. Both biopolymer functionalizations were performed by modification of ε-amine groups present at the side chain of lysines, as described in materials and methods section. The characterization of RGD-N3 and RGD-CO was carried out by ^{1}H-NMR spectroscopy, MALDI-ToF mass spectrometry and FTIR-ATR (see supporting information).

The presence of twenty-four lysine residues distributed along the aminoacidic chain of RGD biopolymer allowed performing amidation reaction of their amine groups with an N-succinimidyl carbonate derivative as a cyclooctyne carrier, giving rise to the RGD-CO biopolymer bearing cyclooctyne groups distributed along the ELR chain. Thirteen lysines from the total were modified when using 0.6 equivalents of reagent, which makes 90% of conversion yield. This conversion was determined by MALDI-ToF and ^{1}H-NMR (in DMSO-d6) analysis that enabled the quantification of the degree of lysine modification (Supporting information). The NMR signals allowed to identify RGD-CO structure (figure S1) and, above all, integral value of H-N hydrogen from new formed carbamate allowed us to quantify the number of amine groups modified. This lysine conversion value is in accordance with the molecular weight increase recorded by MALDI-ToF spectrometry of RGD-CO (figure S2).

In a similar amidation reaction, using 0.6 equivalents of an N-succinimidyl carbonate carrying azide group, RGD was chemically modified to achieve RGD-N3. In this process, fourteen lysines of the total were modified, meaning that 97% of conversion was obtained. The number of lysines modified was calculated as explained above for RGD-CO (figure S3 and S4 for ^{1}H-NMR and MALDI-ToF, respectively) but, in this case, the appearance of a new band at 2100 cm$^{-1}$ in FTIR-ATR spectrum corroborates the presence of azide groups at the biopolymer chain of RGD-N3 (figure S5).

Once optimized the time of PVDF membrane activation with plasma treatment and once the biopolymers were adequately modified to achieve RGD-N3 and RGD-CO, PVDF membrane coating process optimization was carried out following the coating methodology described in materials and methods. In order to study the influence of ELRs solution concentration for the best coating, layer-by-layer assays were performed at different RGD-CO and RGD-N3 solution concentration; in fact, recombinamers were dissolved to achieve 10 and 25 mg/mL solutions (Table 1). On the other hand, as the membranes were sequentially immersed in the ELR solutions, the influence of the order of deposition of the first layer was also evaluated. So, four different types of coated membranes, a-d, were obtained (see Table 1). The verification of the best coating was performed by weight difference between uncoated and coated membranes per square centimetre as well as by water contact angle measurement (Table 1). As it is shown in table 1, the largest increases in weight occurred for membrane types a and b that were firstly coated by RGD-N3, finishing the second bilayer with RGD-CO; and the best of both coatings happened when using the most concentrated solution of 25 mg/mL in membrane b. Moreover, the coating verification by contact angle values showed a lower hydrophobicity for the same membranes a and b, respect to membranes c and d, what is also consistent with a better coating of membranes a and b, being

optimized for membrane b with the lowest contact angle value. These results are also in accordance with the FTIR-ATR recorded for membranes a-d (Figure S6).

**Table 1.** Parameters measured for different coatings on PVDF membranes to optimize coating protocol

| Sample | First layer | Concentration (mg/mL) | $\Delta$P/S (mg/cm$^2$) | Contact Angle (°) |
|---|---|---|---|---|
| a | RGD-N3 | 10 | 0.51 | $77.1 \pm 3.2$ |
| b | RGD-N3 | 25 | 1.10 | $71.1 \pm 1.1$ |
| c | RGD-CO | 10 | 0.06 | $92.3 \pm 5.7$ |
| d | RGD-CO | 25 | 0.28 | $89.9 \pm 6.1$ |

In figure S6, the coated membranes spectrum showed the signals corresponding to ELRs primarily characterized by absorption bands at 3300 and 1700 cm$^{-1}$, corresponding both to N-H and C=O amidic bonds present at the main chain of ELRs, together with the characteristic absorption bands of PVDF membranes before-mentioned in figure 2 with bands ranging from 1300 to 500 cm$^{-1}$. Among the four types of membranes FTIR-ATR spectra, the biggest absorption bands at 1700 cm$^{-1}$, comparing with the ones of PVDF, took place for membranes types a and b.

The structure and morphology of the coating combinations on the PVDF membranes were also characterized by FESEM (figure S7), confirming the results previously obtained by FTIR-ATR, difference in weight and measurements of water contact angle. Sample b coating method, coated with 25 mg/mL solutions of ELRs being RGD-N3 the layer firstly deposited, was chosen as the best to perform cell culture assays. An illustration of the optimized layer-by-layer protocol is depicted in figure 4.
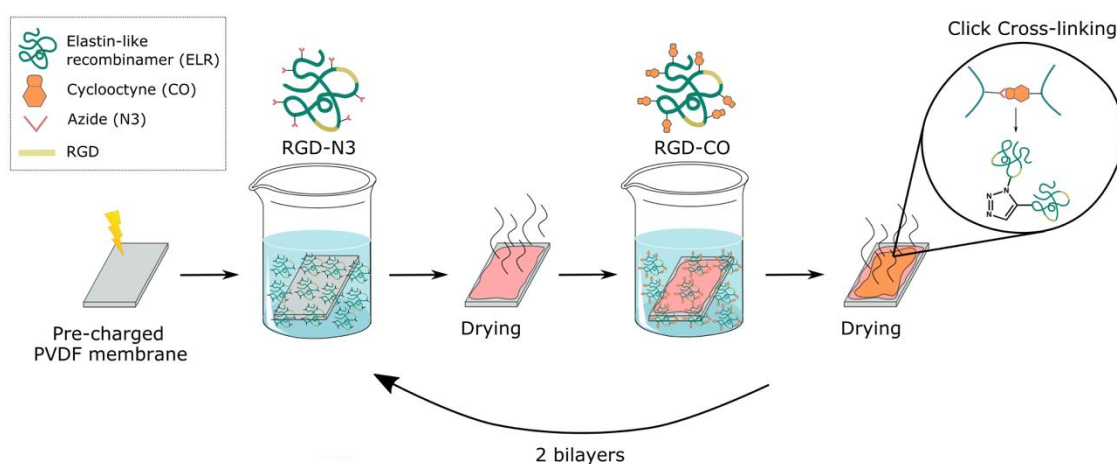


**Figure 4.** Illustration of the optimized layer-by-layer process with RGD-N3 (as first layer) and RGD-CO ELRs onto plasma treated PVDF membranes.

The characterization of the optimized layer-by-layer protocol is shown in figure 5. Figure 5 (a) shows the FTIR-ATR spectra of the coated and non-coated membranes, where the peaks corresponding to the ELRs presence at about 1700 $cm^{-1}$ and 3300 $cm^{-1}$ can be appreciated, reconfirming the best LbL coating method. Images of water contact angles before and after coating are also shown in figure 5 (b), confirming the reduction of hydrophobicity. This reduction in hydrophobicity was also accompanied by a reduction in the surface roughness, as shown in Figure 1. Both surface and cross-section FESEM images show the porous structure of the type b

membranes, but at the cross-section image we can verify the right membrane coating with a thin film covering homogeneously the membrane surface.
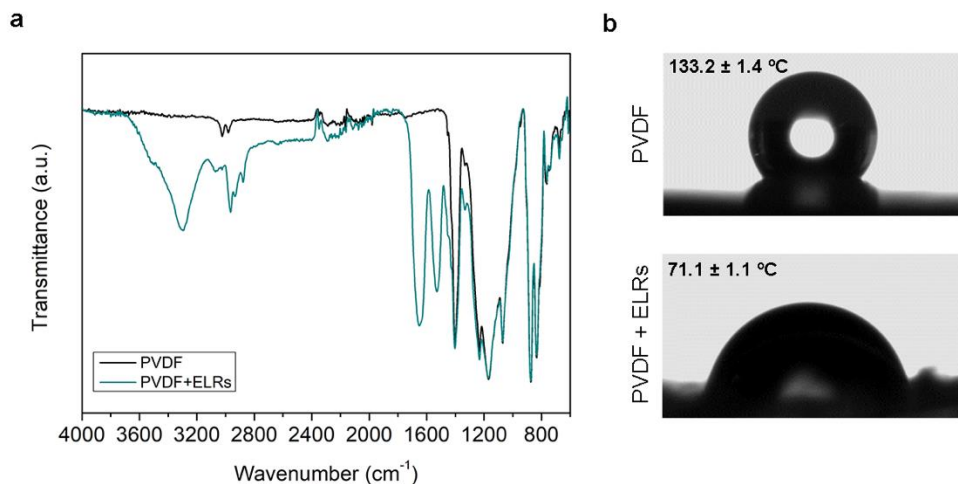


F**igure 5**. (a) Comparison of FTIR-ATR spectra from coated membrane (blue line), specifically type b, and non-coated membrane (black line) and (b) images of their contact angle measurements before (PVDF) and after (PVDF + ELRs) deposition of ELRs applying the optimized protocol.

## 3.3 pMSC response to ELRs layer-by-layer coating

Porcine mesenchymal stem cells were used to test initial cell adhesion and proliferation in PVDF membranes coated by LbL with ELRs or traditionally coated with adsorbed fibronectin. A glass slide coated with fibronectin was also used as standard control. Nuclei-cytoplasm staining at 24 h, 3 and 7 days was evaluated, as reported in figure 6.

Figure 6 (a) shows that after 24 h cells had adhered in all the surfaces, showing an extended cytoskeleton in every condition. Despite this well-developed cytoskeleton, the differences in cell number between conditions are significant. PVDF membranes coated with fibronectin showed a

negative fold change in cell proliferation, meaning that a lower number of cells than the initial cell seeding density had attached on the surface. While in the PVDF + ELRs condition cells had adhered and some of them had even proliferated after 24 h, as shown in figure 6 (b), the initial adhesion in PVDF is really poor, not being even able to retain the initial number of seeded cells.

At longer term, after 7 days, difference in terms of proliferation is noticeable. PVDF + ELRs and glass slide have reached confluence. PVDF coated with fibronectin shows a scarce number of cells after this period of time, even if cells are proliferating, proliferation rate is slow, not reaching the levels displayed by the rest of conditions.
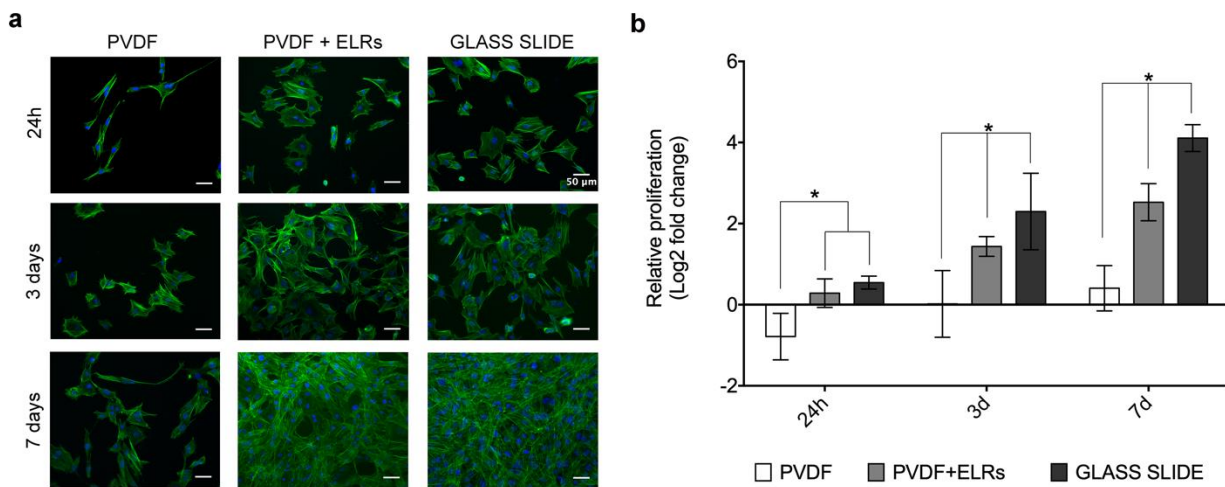


**Figure 6.** (a) Representative images of actin (cytoplasm-green) and DAPI (nucleus-blue) staining after 24 h, 3 and 7 days of culture for coated and uncoated PVDF membranes and glass slide control. Scale bar is 50 μm. (b) Cell count based on the analysis of 4 images taken of the 3 replicates per condition at 24 h, 3 and 7 days, from two independent assays. * $p\text{-}value < 0.05$

Hydrophobicity is a key feature in PVDF, as demonstrated by PVDF membrane contact angle before coating (133.2 ± 1.4 º). This effect is largely increased by the surface roughness present in the membranes due to the spherulitic conformation.

This characteristic makes surface treatments an unavoidable approach for cell culture on PVDF. Since this polymer began to be used in the tissue engineering field it has been traditionally coated with fibronectin [8,19,20]. In this work, fibronectin adsorption was not enough to promote initial cell adhesion in PVDF microporous membranes. This type of coating has previously been proven to be inefficient in spherulitic-like PVDF membranes [21]. Previous results of our group indicate that small changes in porosity degree in fibronectin coated PVDF membranes can influence initial cell adhesion and proliferation in porcine bone marrow mesenchymal stem cells.

Contact angle is closely related with polymer wettability but also with surface roughness. Layer by layer deposition of elastin-like recombinamers reduced water contact angle value in PVDF membranes (71.1 ± 1.1 º) partially due to surface smoothing. The presence of RGD sequences in the ELRs and its deposition by LbL, which flatted membrane's surface, increased initial pMSC adhesion in PVDF + ELRs membranes. Combination of both features make this coating a suitable option for mesenchymal stem cell culture on porous PVDF membranes.

These findings lead the way to the use of PVDF membranes coated with elastin-like recombinamers containing RGD sequences in future MSC differentiation approaches towards the osteogenic lineage.

### 4. CONCLUSIONS

Non-solvent induced phase separation has proven to be a cost-effective and reliable technique for manufacturing PVDF membranes. The use of ethanol as non-solvent produced homogeneously porous membranes with a percentage of γ-phase greater than 90 % and an overall crystalline content up to 66 %. Its electroactive potential was confirmed, after poling by contact method, measuring the d33 piezeoelectric coefficient, obtaining values comprised in the bone piezoelectricity range. Membranes were coated with elastin-like recombinamers containing RGD sequences to improve its initial cell adhesion properties. ELRs were deposited by layer-by-layer technique applying the click cross-linking chemistry. After coating optimization, modified ELRs containing azide groups were selected to be deposited as first layer, followed by ELRs modified to contain cyclooctyne groups. Both layers reacted by interchain crosslinking via catalyst-free Hüisgen 1,3-dipolar cycloaddition, generating a stable bilayer. Two bilayers were deposited, reducing surface roughness and contact angle. Cell adhesion and proliferation was tested using porcine bone marrow MSCs in a short-term culture (1 to 7 days). ELRs deposition by LbL was compared to traditional fibronectin adsorption, showing that cells preferred ELRs coated surfaces regarding initial adhesion and proliferation. Fibronectin adsorption showed poor cell attachment, not being able to retain the initial number of seeded cells, while ELRs favored adhesion and enhanced proliferation after 7 days. These findings open the door for the combination of electroactive PVDF membranes and synthetic peptides containing biofunctional sequences for mesenchymal stem cell culture and differentiation towards the osteogenic lineage.

**SUPPORTING INFORMATION**

Supplementary data associated with this article can be found in SI: 1H-NMR, MALDI-ToF and FTIR-ATR of RGD-CO and RGD-N3 for structure characterization of modified biopolymers; and FTIR-ATR and FESEM images of PVDF coated and non-coated membranes for stablishing optimal conditions.

## REFERENCES

(1)     Lovinger, A. J. Annealing of Poly(Vinylidene Fluoride) and Formation of a Fifth Phase.

*Macromolecules* **1982**, *15* (1), 40–44. https://doi.org/10.1021/ma00229a008.

(2)     Martins, P.; Lopes, A. C.; Lanceros-Mendez, S. Electroactive Phases of Poly(Vinylidene Fluoride): Determination, Processing and Applications. *Prog. Polym. Sci.* **2014**, *39* (4), 683–706. https://doi.org/10.1016/j.progpolymsci.2013.07.006.

(3)     Jacob, J.; More, N.; Kalia, K.; Kapusetti, G. Piezoelectric Smart Biomaterials for Bone and Cartilage Tissue Engineering. *Inflamm. Regen.* **2018**, *38* (1), 1–11. https://doi.org/10.1186/s41232-018-0059-8.

(4)     Fukada, E.; Yasuda, I. On the Piezoelectric Effect of Bone. *J. Phys. Soc. Japan* **1957**, *12* (10), 1158–1162.

(5)     Ahn, A. C.; Alan J. Grodzinsky. Relevance of Collagen Piezoelectricity to "Wolff's Law": A Critical Review. **2010**, *31* (7), 733–741. https://doi.org/10.1016/j.medengphy.2009.02.006.RELEVANCE.

(6)     Ribeiro, C.; Moreira, S.; Correia, V.; Sencadas, V.; Rocha, J. G.; Gama, F. M.; Gómez Ribelles, J. L.; Lanceros-Méndez, S. Enhanced Proliferation of Pre-Osteoblastic Cells by Dynamic Piezoelectric Stimulation. *RSC Adv.* **2012**, *2* (30), 11504. https://doi.org/10.1039/c2ra21841k.

(7)     Ribeiro, C.; Correia, D. M.; Ribeiro, S.; Sencadas, V.; Botelho, G.; Lanceros-Méndez, S. Piezoelectric Poly(Vinylidene Fluoride) Microstructure and Poling State in Active Tissue Engineering. *Eng. Life Sci.* **2015**, *15* (4), 351–356. https://doi.org/10.1002/elsc.201400144.

(8)     Sobreiro-Almeida, R.; Tamaño-Machiavello, M.; Carvalho, E.; Cordón, L.; Doria, S.;

Senent, L.; Correia, D.; Ribeiro, C.; Lanceros-Méndez, S.; Sabater i Serra, R.; Gomez Ribelles, J.; Sempere, A. Human Mesenchymal Stem Cells Growth and Osteogenic Differentiation on Piezoelectric Poly(Vinylidene Fluoride) Microsphere Substrates. *Int. J. Mol. Sci.* **2017**, *18* (11), 2391. https://doi.org/10.3390/ijms18112391.

(9) Gregorio, R. Determination of the α, β, and γ Crystalline Phases of Poly(Vinylidene Fluoride) Films Prepared at Different Conditions. *J. Appl. Polym. Sci.* **2006**, *100* (4), 3272–3279. https://doi.org/10.1002/app.23137.

(10) Sencadas, V.; Gregorio, R.; Lanceros-Méndez, S. α to β Phase Transformation and Microstructural Changes of PVDF Films Induced by Uniaxial Stretch. *J. Macromol. Sci. Part B Phys.* **2009**, *48* (3), 514–525. https://doi.org/10.1080/00222340902837527.

(11) Pagliero, M.; Bottino, A.; Comite, A.; Costa, C. Novel Hydrophobic PVDF Membranes Prepared by Nonsolvent Induced Phase Separation for Membrane Distillation. *J. Memb. Sci.* **2020**, *596* (September 2019). https://doi.org/10.1016/j.memsci.2019.117575.

(12) Boccaccio, T.; Bottino, A.; Capannelli, G.; Piaggio, P. Characterization of PVDF Membranes by Vibrational Spectroscopy. *J. Memb. Sci.* **2002**, *210* (2), 315–329. https://doi.org/10.1016/S0376-7388(02)00407-6.

(13) Ribeiro, C.; Costa, C. M.; Correia, D. M.; Nunes-Pereira, J.; Oliveira, J.; Martins, P.; Gonçalves, R.; Cardoso, V. F.; Lanceros-Méndez, S. Electroactive Poly(Vinylidene Fluoride)-Based Structures for Advanced Applications. *Nat. Protoc.* **2018**, *13* (4), 681–704. https://doi.org/10.1038/nprot.2017.157.

(14) Wang, X.; Zhang, L.; Sun, D.; An, Q.; Chen, H. Formation Mechanism and Crystallization

of Poly(Vinylidene Fluoride) Membrane via Immersion Precipitation Method. *Desalination* **2009**, *236* (1–3), 170–178. https://doi.org/10.1016/j.desal.2007.10.064.

(15) Cheng, L. P. Effect of Temperature on the Formation of Microporous PVDF Membranes by Precipitation from 1-Octanol/DMF/PVDF and Water/ DMF/PVDF Systems. *Macromolecules* **1999**, *32* (20), 6668–6674. https://doi.org/10.1021/ma990418l.

(16) Liu, F.; Hashim, N. A.; Liu, Y.; Abed, M. R. M.; Li, K. Progress in the Production and Modification of PVDF Membranes. *J. Memb. Sci.* **2011**, *375* (1–2), 1–27. https://doi.org/10.1016/j.memsci.2011.03.014.

(17) Guillot-Ferriols, M.; Rodríguez-Hernández, J. C.; Correia, D. M.; Carabineiro, S. A. C.; Lanceros-Méndez, S.; Gómez Ribelles, J. L.; Gallego Ferrer, G. Poly(Vinylidene ) Fluoride Membranes Coated by Heparin / Collagen Layer-by-Layer, Smart Biomimetic Approaches for Mesenchymal Stem Cell Culture. *Mater. Sci. Eng. C* **2020**, *117*, 111281. https://doi.org/10.1016/j.msec.2020.111281.

(18) Webb, K.; Hlady, V.; Tresco, P. A. Relative Importance of Surface Wettability and Charged Functional Groups on NIH 3T3 Fibroblast Attachment, Spreading, and Cytoskeletal Organization. *J. Biomed. Mater. Res.* **1998**, *41* (3), 422–430. https://doi.org/10.1002/(SICI)1097-4636(19980905)41:3<422::AID-JBM12>3.0.CO;2-K.

(19) Ribeiro, C.; Panadero, J. A.; Sencadas, V.; Lanceros-M??ndez, S.; Tama??o, M. N.; Moratal, D.; Salmer??n-S??nchez, M.; G??mez Ribelles, J. L. Fibronectin Adsorption and Cell Response on Electroactive Poly(Vinylidene Fluoride) Films. *Biomed. Mater.* **2012**, *7* (3). https://doi.org/10.1088/1748-6041/7/3/035004.

(20) Ribeiro, C.; Pärssinen, J.; Sencadas, V.; Correia, V.; Miettinen, S.; Hytönen, V. P.; Lanceros-Méndez, S. Dynamic Piezoelectric Stimulation Enhances Osteogenic Differentiation of Human Adipose Stem Cells. *J. Biomed. Mater. Res. - Part A* **2015**, *103* (6), 2172–2175. https://doi.org/10.1002/jbm.a.35368.

(21) Morales-Román, R. M.; Guillot-Ferriols, M.; Roig-Pérez, L.; Lanceros-Mendez, S.; Gallego-Ferrer, G.; Gómez Ribelles, J. L. Freeze-Extraction Microporous Electroactive Supports for Cell Culture. *Eur. Polym. J.* **2019**, *119* (June), 531–540. https://doi.org/10.1016/j.eurpolymj.2019.07.011.

(22) Rodríguez-Cabello, J. C.; Martín, L.; Alonso, M.; Arias, F. J.; Testera, A. M. "Recombinamers" as Advanced Materials for the Post-Oil Age. *Polymer (Guildf).* **2009**, *50* (22), 5159–5169. https://doi.org/10.1016/j.polymer.2009.08.032.

(23) Girotti, A.; Reguera, J.; Rodríguez-Cabello, J. C.; Arias, F. J.; Alonso, M.; Testera, A. M. Design and Bioproduction of a Recombinant Multi(Bio)Functional Elastin-like Protein Polymer Containing Cell Adhesion Sequences for Tissue Engineering Purposes. *J. Mater. Sci. Mater. Med.* **2004**, *15* (4), 479–484. https://doi.org/10.1023/B:JMSM.0000021124.58688.7a.

(24) Berg, M. C.; Yang, S. Y.; Hammond, P. T.; Rubner, M. F. Controlling Mammalian Cell Interactions on Patterned Polyelectrolyte Multilayer Surfaces. *Langmuir* **2004**, *20* (4), 1362–1368. https://doi.org/10.1021/la0355489.

(25) Ruoslahti, E. RGD and Other Recognition Sequences for Integrins. *Annu. Rev. Cell Dev. Biol.* **1996**, *12* (1), 697–715. https://doi.org/10.1146/annurev.cellbio.12.1.697.

(26) Nicol, A.; Channe Gowda, D.; Urry, D. W. Cell Adhesion and Growth on Synthetic Elastomeric Matrices Containing ARG-GLY–ASP–SER–3. *J. Biomed. Mater. Res.* **1992**, *26* (3), 393–413. https://doi.org/10.1002/jbm.820260309.

(27) Costa, R. R.; Custódio, C. A.; Testera, A. M.; Arias, F. J.; Rodríguez-Cabello, J. C.; Alves, N. M.; Mano, J. F. Stimuli-Responsive Thin Coatings Using Elastin-like Polymers for Biomedical Applications. *Adv. Funct. Mater.* **2009**, *19* (20), 3210–3218. https://doi.org/10.1002/adfm.200900568.

(28) Qu, Z.; Yan, J.; Li, B.; Zhuang, J.; Huang, Y. Improving Bone Marrow Stromal Cell Attachment on Chitosan/Hydroxyapatite Scaffolds by an Immobilized RGD Peptide. *Biomed. Mater.* **2010**, *5* (6). https://doi.org/10.1088/1748-6041/5/6/065001.

(29) Yang, F.; Williams, C. G.; Wang, D. A.; Lee, H.; Manson, P. N.; Elisseeff, J. The Effect of Incorporating RGD Adhesive Peptide in Polyethylene Glycol Diacrylate Hydrogel on Osteogenesis of Bone Marrow Stromal Cells. *Biomaterials* **2005**, *26* (30), 5991–5998. https://doi.org/10.1016/j.biomaterials.2005.03.018.

(30) Shin, H.; Temenoff, J. S.; Bowden, G. C.; Zygourakis, K.; Farach-Carson, M. C.; Yaszemski, M. J.; Mikos, A. G. Osteogenic Differentiation of Rat Bone Marrow Stromal Cells Cultured on Arg-Gly-Asp Modified Hydrogels without Dexamethasone and β-Glycerol Phosphate. *Biomaterials* **2005**, *26* (17), 3645–3654. https://doi.org/10.1016/j.biomaterials.2004.09.050.

(31) Anderson, J. M.; Vines, J. B.; Patterson, J. L.; Chen, H.; Javed, A.; Jun, H.-W. Osteogenic Differentiation of Human Mesenchymal Stem Cells Synergistically Enhanced by

Biomimetic Peptide Amphiphiles Combined with Conditioned Medium. *Acta Biomater.* **2012**, *7* (2), 675–682. https://doi.org/10.1016/j.actbio.2010.08.016.Osteogenic.

(32)   González De Torre, I.; Santos, M.; Quintanilla, L.; Testera, A.; Alonso, M.; Rodríguez Cabello, J. C. Elastin-like Recombinamer Catalyst-Free Click Gels: Characterization of Poroelastic and Intrinsic Viscoelastic Properties. *Acta Biomater.* **2014**, *10* (6), 2495–2505. https://doi.org/10.1016/j.actbio.2014.02.006.

(33)   Nettles, D. L.; Chilkoti, A.; Setton, L. A. Applications of Elastin-like Polypeptides in Tissue Engineering. *Adv. Drug Deliv. Rev.* **2010**, *62* (15), 1479–1485. https://doi.org/10.1016/j.addr.2010.04.002.

(34)   Sousa, M. P.; Gonzalez de Torre, I.; Oliveira, M. B.; Rodríguez-Cabello, J. C.; Mano, J. F. Biomimetic Click Assembled Multilayer Coatings Exhibiting Responsive Properties. *Mater. Today Chem.* **2017**, *4*, 150–163. https://doi.org/10.1016/j.mtchem.2017.04.001.

(35)   Benz, M.; Euler, W. B. Determination of the Crystalline Phases of Poly(Vinylidene Fluoride) under Different Preparation Conditions Using Differential Scanning Calorimetry and Infrared Spectroscopy. *J. Appl. Polym. Sci.* **2003**, *89* (4), 1093–1100. https://doi.org/10.1002/app.12267.

(36)   Chang, H. H.; Chang, L. K.; Yang, C. D.; Lin, D. J.; Cheng, L. P. Effect of Polar Rotation on the Formation of Porous Poly(Vinylidene Fluoride) Membranes by Immersion Precipitation in an Alcohol Bath. *J. Memb. Sci.* **2016**, *513*, 186–196. https://doi.org/10.1016/j.memsci.2016.04.052.

(37)   Lopes, A. C.; Costa, C. M.; Tavares, C. J.; Neves, I. C.; Lanceros-Mendez, S. Nucleation

of the Electroactive γ Phase and Enhancement of the Optical Transparency in Low Filler Content Poly(Vinylidene)/Clay Nanocomposites. *J. Phys. Chem. C* **2011**, *115* (37), 18076–18082. https://doi.org/10.1021/jp204513w.

(38)    Nakagawa, K.; Ishida, Y. Annealing Effects in Poly(Vinylidene Fluoride) as Revealed by Specific Volume Measurements, Differential Scanning Calorimetry, and Electron Microscopy. *J. Polym. Sci. Part A-2 Polym. Phys.* **1973**, *11* (11), 2153–2171. https://doi.org/10.1002/pol.1973.180111107.

(39)    Pinedo-Martín, G.; Santos, M.; Testera, A. M.; Alonso, M.; Rodríguez-Cabello, J. C. The Effect of NaCl on the Self-Assembly of Elastin-like Block Co-Recombinamers: Tuning the Size of Micelles and Vesicles. *Polymer (Guildf).* **2014**, *55* (21), 5314–5321. https://doi.org/10.1016/j.polymer.2014.08.053.

(40)    Meyer, D. E.; Chilkoti, A. Purification of Recombinant Proteins by Fusion with Thermally-Responsive Polypeptides. *Nat. Biotechnol.* **1999**, *17* (11), 1112–1115. https://doi.org/10.1038/15100.

(41)    Girotti, A.; Orbanic, D.; Ibáñez-Fonseca, A.; Gonzalez-Obeso, C.; Rodríguez-Cabello, J. C. Recombinant Technology in the Development of Materials and Systems for Soft-Tissue Repair. *Adv. Healthc. Mater.* **2015**, *4* (16), 2423–2455. https://doi.org/10.1002/adhm.201500152.

(42)    Jung, J. T.; Kim, J. F.; Wang, H. H.; di Nicolo, E.; Drioli, E.; Lee, Y. M. Understanding the Non-Solvent Induced Phase Separation (NIPS) Effect during the Fabrication of Microporous PVDF Membranes via Thermally Induced Phase Separation (TIPS). *J. Memb.*

*Sci.* **2016**, *514*, 250–263. https://doi.org/10.1016/j.memsci.2016.04.069.

(43)   Lin, D. J.; Beltsios, K.; Young, T. H.; Jeng, Y. S.; Cheng, L. P. Strong Effect of Precursor Preparation on the Morphology of Semicrystalline Phase Inversion Poly(Vinylidene Fluoride) Membranes. *J. Memb. Sci.* **2006**, *274* (1–2), 64–72. https://doi.org/10.1016/j.memsci.2005.07.043.

(44)   Lin, D. J.; Beltsios, K.; Chang, C. L.; Cheng, L. P. Fine Structure and Formation Mechanism of Particulate Phase-Inversion Poly(Vinylidene Fluoride) Membranes. *J. Polym. Sci. Part B Polym. Phys.* **2003**, *41* (13), 1578–1588. https://doi.org/10.1002/polb.10513.

(45)   Martins, P.; Lopes, A. C.; Lanceros-Mendez, S. Electroactive Phases of Poly(Vinylidene Fluoride): Determination, Processing and Applications. *Prog. Polym. Sci.* **2014**, *39* (4), 683–706. https://doi.org/10.1016/j.progpolymsci.2013.07.006.

(46)   Chang, H. H.; Chang, L. K.; Yang, C. D.; Lin, D. J.; Cheng, L. P. Effect of Solvent on the Dipole Rotation of Poly(Vinylidene Fluoride) during Porous Membrane Formation by Precipitation in Alcohol Baths. *Polymer (Guildf).* **2017**, *115*, 164–175. https://doi.org/10.1016/j.polymer.2017.03.044.

(47)   Kim, K. M.; Jeon, W. S.; Park, N. G.; Ryu, K. S.; Chang, S. H. Effect of Evaporation Temperature on the Crystalline Properties of Solution-Cast Films of Poly(Vinylidene Fluoride)S. *Korean J. Chem. Eng.* **2003**, *20* (5), 934–941. https://doi.org/10.1007/BF02697302.

(48)   Lizundia, E.; Reizabal, A.; Costa, C. M.; Maceiras, A.; Lanceros-Méndez, S. Electroactive γ-Phase, Enhanced Thermal and Mechanical Properties and High Ionic Conductivity

Response of Poly (Vinylidene Fluoride)/Cellulose Nanocrystal. *Materials (Basel).* **2020**, *13* (3), 743. https://doi.org/doi:10.3390/ma13030743.

(49)    Salimi, A.; Yousefi, A. A. Conformational Changes and Phase Transformation Mechanisms in PVDF Solution-Cast Films. *J. Polym. Sci. Part B Polym. Phys.* **2004**, *42* (18), 3487–3495. https://doi.org/10.1002/polb.20223.

(50)    Gonçalves, S.; Serrado-Nunes, J.; Oliveira, J.; Pereira, N.; Hilliou, L.; Costa, C. M.; Lanceros-Méndez, S. Environmentally Friendly Printable Piezoelectric Inks and Their Application in the Development of All-Printed Touch Screens. *ACS Appl. Electron. Mater.* **2019**, *1* (8), 1678–1687. https://doi.org/10.1021/acsaelm.9b00363.

(51)    Liboff, A. R.; Furst, M. Pyroelectric Effect in Collagenous Structures. *Ann. N. Y. Acad. Sci.* **1974**, *238* (1), 26–35. https://doi.org/10.1111/j.1749-6632.1974.tb26777.x.

(52)    Fukada, E. Mechnical Deformation and Electrical Polarization in Biological Substances. *Biorheology* **1968**, *5* (3), 199–208. https://doi.org/10.3233/BIR-1968-5302.

(53)    Fukada, E.; Yasuda, I. Piezoelectric Effects in Collagen. *Japanese J. Appl. Physics, Part 1 Regul. Pap. Short Notes Rev. Pap.* **1964**, *3* (8), 502B. https://doi.org/10.1143/jjap.3.502b.

(54)    Lang, S. B. Piezoelectricity, Pyroelectricity and Ferroelectricity in Biomaterials: Speculation on Their Biological Significance. *IEEE Trans. Dielectr. Electr. Insul.* **2000**, *7* (4), 466–473. https://doi.org/10.1109/94.868063.

(55)    Halperin, C.; Mutchnik, S.; Agronin, A.; Molotskii, M.; Urenski, P.; Salai, M.; Rosenman, G. Piezoelectric Effect in Human Bones Studied in Nanometer Scale. *Nano Lett.* **2004**, *4*

(7), 1253–1256. https://doi.org/10.1021/nl049453i.

(56)    De Torre, I. G.; Wolf, F.; Santos, M.; Rongen, L.; Alonso, M.; Jockenhoevel, S.; C.Rodríguez-Cabello, J.; Mela, P. Elastin-like Recombinamer-Covered Stents: Towards a Fully Biocompatible and Non-Thrombogenic Device for Cardiovascular Diseases. *Acta Biomater.* **2015**, *12* (1), 146–155. https://doi.org/10.1016/j.actbio.2014.10.029.